Reactions of Hydrogen Atom with Hydrogen Peroxide

5 AUTHORS, INCLUDING:

Benjamin A Ellingson
OpenEye Scientific Software

10 PUBLICATIONS **632** CITATIONS

SEE PROFILE

Jingjing Zheng
Gaussian, Inc.

53 PUBLICATIONS **1,800** CITATIONS

SEE PROFILE

Donald Truhlar
University of Minnesota Twin Cities

1,342 PUBLICATIONS **81,415** CITATIONS

SEE PROFILE

Reactions of Hydrogen Atom with Hydrogen Peroxide

Benjamin A. Ellingson, Daniel P. Theis,[†] Oksana Tishchenko, Jingjing Zheng, and Donald G. Truhlar*

Department of Chemistry and Supercomputing Institute, University of Minnesota, 207 Pleasant Street SE, Minneapolis, Minnesota 55455-0431

Received: September 13, 2007; In Final Form: October 12, 2007

Rate coefficients are calculated using canonical variational transition state theory with multidimensional tunneling (CVT/SCT) for the reactions $H + H_2O_2 \rightarrow H_2O + OH$ (1a) and $H + H_2O_2 \rightarrow HO_2 + H_2$ (1b). Reaction barrier heights are determined using two theoretical approaches: (i) comparison of parametrized rate coefficient calculations employing CVT/SCT to experiment and (ii) high-level *ab initio* methods. The evaluated experimental data reveal considerable variations of the barrier height for the first reaction: although the zero-point-exclusive barrier for (1a) derived from the data by Klemm *et al.* (*First Int. Chem. Kinet. Symposium* 1975, 61) is 4.6 kcal/mol, other available measurements result in a higher barrier of 6.2 kcal/mol. The empirically derived zero-point-exclusive barrier for (1b) is 10.4 kcal/mol. The electronic structure of the system at transition state geometries in both reactions was found to have "multireference" character; therefore special care was taken when analyzing electronic structure calculations. Transition state geometries are optimized by multireference perturbation theory (MRMP2) with a variety of one-electron basis sets, and by a multireference coupled cluster (MR-AQCCSD) method. A variety of single-reference benchmark-level calculations have also been carried out; included among them are BMC-CCSD, G3SX(MP3), G3SX, G3, G2, MCG3, CBS-APNO, CBS-Q, CBS-QB3, and CCSD(T). Our data obtained at the MRMP2 level are the most complete; the barrier height for (1a) using MRMP2 at the infinite basis set limit is 4.8 kcal/mol. Results are also obtained with midlevel single-reference multicoefficient correlation methods, such as MC3BB, MC3MPW, MC-QCISD/3, and MC-QCISD-MPWB, and with a variety of hybrid density functional methods, which are compared with high-level theory. On the basis of the evaluated experimental values and the benchmark calculations, two possible recommended values are given for the rate coefficients.

1. Introduction

Due to the rising cost of gasoline and growing concern about the rapid rate of oil consumption, a significant amount of research has been performed to identify alternate sources of energy.[1–3] One alternative fuel that is being considered is hydrogen gas. Hydrogen gas offers a clean source of fuel that can produce a reasonable amount of energy and can be chemically synthesized from renewable resources at an affordable cost.[1] These characteristics have led several researchers to study the feasibility of developing a combustion engine that uses H_2 for fuel.[3] This in turn has resulted in a renewed interest in the details of H_2/O_2 combustion.[4] In addition, it has long been known that the oxidation of H_2 makes a significant contribution to the later stages of hydrocarbon oxidation.[5,6]

Two reactions that play an important role in the high-temperature, high-pressure behavior of the H_2/O_2 combustion system are[5–14]

$$H + H_2O_2 \rightarrow H_2O + OH \qquad (1a)$$

$$H + H_2O_2 \rightarrow HO_2 + H_2 \qquad (1b)$$
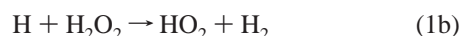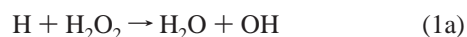
These reactions influence the dependence of the second explosion limit[8] on temperature and reactant concentration and

dependence of the maximum rate of non-explosive oxidation on the pressure, temperature, and reactant concentration.[7,9] A recent study also found that for experimental conditions (pressures, temperatures, etc.) above the third explosion limit these reactions affect the length of time it takes to autocatalytically induce an explosion.[4]

Unfortunately, low-temperature measurements of the rate coefficients k_{1a} and k_{1b} of reactions 1a and 1b and of the sum of these two rate coefficients (which is denoted k_1) have shown significant variations both in the absolute magnitude of total rate coefficient k_1 and in the branching ratio R, defined as the rate of reaction 1a relative to the rate of reaction 1b, k_{1a}/k_{1b}.[15–18] These reactions have been difficult to study because they involve the same reactants, because OH can react with H_2O_2 as a second route to producing H_2O, and because HO_2 can react with H to produce either H_2 or H_2O. Reaction 1b has also been studied recently using single-reference and multireference perturbation theories and using density functional theory; these calculations led to an estimate of 8.1–9.3 kcal/mol for the barrier height of this reaction.[19,20]

In this Article, two complementary theoretical approaches have been employed to estimate the reaction barriers for reactions 1a and 1b. These approaches are (i) comparison of parametrized rate coefficient calculations employing canonical variational theory with small-curvature tunneling[21–25] (CVT/SCT) to experiments and (ii) high-level electronic structure calculations, such as the benchmark-level multicoefficient correlation methods and the multireference correlation methods

---

* Corresponding author. E-mail: truhlar@umn.edu.
† Current address: Chemistry Department, University of North Dakota, 151 Cornell St., Stop 9024, Grand Forks, ND 58202.

Reactions of H Atom with Hydrogen Peroxide

J. Phys. Chem. A, Vol. 111, No. 51, 2007 **13555**

(MRCMs). Additionally, results obtained using midlevel multicoefficient correlation methods and hybrid density functional theory (HDFT) are included for comparison.

2. Computational Methods

2.1. Dynamics Methods. All rate coefficient calculations were performed using variational transition state theory based on direct dynamics[26-33] with GAUSSRATE version 9.6.[34] Direct dynamics calculations are based on an implicit potential energy surface produced by "on the fly" electronic structure calculations; for the present calculations, GAUSSRATE interfaces the *Gaussian 03* electronic structure package[35] with POLYRATE version 9.6.[36] The variational transition state theory rate coefficients are calculated by canonical variational theory[21-25] (CVT) with a transmission coefficient. The transmission coefficient includes the effects of quantum-mechanical tunneling and nonclassical reflection by the centrifugal-dominant small-curvature semiclassical ground state approximation,[23-25] CD-SCSAG, which is henceforth abbreviated as SCT, which denotes small-curvature tunneling. The CD-SCSAG method is multidimensional in two ways: (i) the effective potential for tunneling depends on the vibrational force coefficients of many degrees of freedom orthogonal to the reaction path; (ii) the tunneling path is multidimensional and differs from the minimum energy path in many degrees of freedom.

Two types of CVT/SCT calculations were carried out: single-level and dual-level. Except where stated otherwise, all dynamics calculations are straight direct dynamics calculations[26,30] in which all energies, gradients, and Hessians are evaluated consistently at a single electronic-structure level without fitting. The dual-level calculations are carried out by the interpolated single-point energies (VTST-ISPE) scheme,[37] which uses a spline-under-tension curve fitting to adjust the potential energy along the minimum energy path calculated at a particular electronic structure level to agree with higher-level estimates or trial values of the barrier height and energy of reaction. The VTST-ISPE scheme is described in detail elsewhere.[37]

For all the rate calculations, the $C\omega$ torsional anharmonicity scheme[38a] was applied to the torsional vibrational mode of the H_2O_2 reactant and to the generalized transition states. Both the reduced moment of inertia for the internal rotation and the effective torsional potential energy function depend on the position along the reaction coordinate. In the $C\omega$ scheme, the reduced moment of inertia for the internal rotation is calculated in internal coordinates by the method of Pitzer[38b] and the force constant of the periodic potential energy function[38c,38d] for the internal rotation is adjusted to match the harmonic frequency obtained by normal-mode analysis of the reactant and generalized normal-mode analysis of the generalized transition states. This scheme was selected on the basis of previous tests[38a] of various anharmonicity schemes for the reactant.

Redundant internal coordinates[39,40] and reorientation of the dividing surface[41] (RODS) have been used. Redundant internal coordinates consist of bond stretches (*str*), valence bends (*vb*), linear bends (*lb*), and torsions (*t*).[38e] For the calculations presented in this paper the coordinates chosen are {*str*12, *str*23, *str*35, *str*34, *vb*123, *vb*235, *vb*234, *vb*534, *t*1235, *t*1234} for reaction 1a and {*str*12, *str*23, *str*34, *str*35, *vb*123, *vb*234, *lb*345, *t*1234, *t*1235} for reaction 1b. These coordinates are shown in Figures 1 and 2, respectively. Because there are ten total coordinates in each case (a linear bend serves as two internal coordinates), whereas only nine are nonredundant for a five-atom system, the coordinates are redundant.[39,40] The RODS scheme involves reorienting the generalized transition state
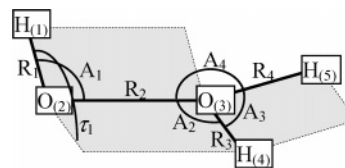
Figure 1. Internal coordinates used to describe the saddle point of reaction 1a.
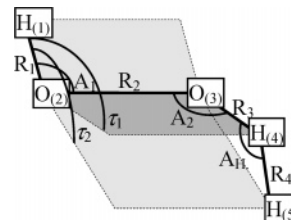
Figure 2. Internal coordinates used to describe the saddle point of reaction 1b.

dividing surface to minimize the quasiclassical flux through it, as described elsewhere.[41]

2.2. Zero-Point Energies. To compare experimentally measured bond dissociation or atomization energies corresponding to 0 K to equilibrium energies obtained using electronic structure methods, the experimental data need to be connected to zero-point-exclusive quantities. The zero-point exclusive energies are the differences in Born–Oppenheimer electronic energies (including nuclear repulsion), and they are related to the experimentally measured counterparts at 0 K by subtracting the zero-point vibrational energies from the latter. The experimental zero-point-exclusive energies of reaction and the experimentally measured bond dissociation energies were determined by the following process: First the experimentally measured heats of formation at 0 K of each reactant and product were used to determine the enthalpies of reaction and the bond dissociation enthalpies at 0 K. Then the best estimates of the change in the zero-point energy in the reaction were subtracted from the enthalpies of the reactions to determine the zero-point-exclusive energies of the reactions. The enthalpies of formation for H, H_2, and H_2O are taken from ref 42. The enthalpies of formation for OH, HO_2, and H_2O_2 are taken from ref 43 and ref 44. The zero-point energy of OH is taken from ref 45. The zero-point energies for H_2O and H_2O_2 were estimated using the harmonic approximation from the frequencies taken from ref 45 and ref 46. The zero-point energy of H_2, HO_2, and H_2O_2 were estimated using the harmonic approximation from the frequencies taken from refs 45, 47, and 48, respectively.

2.3. Electronic Structure Calculations. Because barrier heights cannot be experimentally measured, benchmark-level electronic structure calculations of the forward and reverse barrier heights are used as one way to estimate the barrier heights. Included among the set of benchmark-level electronic structure methods were the G2,[49] G3,[50] G3X,[51] G3SX,[51] and G3SX(MP3)[51] multilevel methods, the CBS-Q,[52] CBS-QB3,[53] and CBS-APNO[52] complete basis set methods, and the MCG3/3[54] and BMC-CCSD[55] multilevel correlation methods. Of these multilevel methods, G3SX, G3SX(MP3), MCG3/3, and BMC-CCSD are multicoefficient correlation methods (MCCMs), and the other methods are other kinds of single-reference (SRML) multilevel methods. MC-QCISD/3[56] optimized geometries were used for all of the benchmark-level multilevel calculations. These calculations were carried out with the *Gaussian 03*[35] and MULTILEVEL[57] codes. The reliability of the high-level electronic structure methods was assessed in several ways. The results of the high-level calculations of the energies of reaction

and the relevant bond energies were compared to experimental measurements to confirm that they accurately describe the energetic nature of the reactions. They were also compared to one another to confirm that they predict consistent values for the barrier heights.

Several diagnostic tests were performed to ascertain the multireference character of the reactions. In a further attempt to explore the effect of multireference character on the energetics and geometries of the transition states, we carried out post-CASSCF calculations, which are also called multireference correlation methods (MRCMs). A necessary preliminary to any CASSCF[58,59] (equivalent to FORS[60]) calculation is the choice of active space (n/m), where n is the number of active electrons and m is the number of active orbitals. Three approaches as to the choice of the active space may be identified, and they will be called the correlating orbital (CO) scheme, the atomic-parentage (AP) scheme, and the natural orbital (NO) scheme. The CO scheme always leads to $m = n$; it involves adding a single correlating orbital to each doubly occupied valence molecular orbital in the active space. Two examples of active spaces built accordingly to this scheme were employed in the present study: (i) a smaller active space (CO:3/3) that consists of bonding and antibonding orbitals of the breaking bond (σ-(OO) and σ*(OO) for reaction 1a and σ(OH) and σ*(OH) for reaction 1b) and the singly occupied molecular orbital (SOMO) that correlates to the 1s orbital of the hydrogen atom at the reactant asymptote of the PES and, depending on the reaction channel, either to the SOMO of the ground electronic state of the OOH radical at the product asymptote 1a or to the SOMO in the ground $X^2\Pi$ state of the OH radical at the product asymptote 1b, and (ii) a larger active space (CO:11/11) constructed by adding a single correlating orbital to each doubly occupied valence molecular orbital that originates from the 2p-(O) and 1s(H) atomic orbitals. The (3/3) active space is the minimal reference space to describe the bond breaking and bond formation in this system, because it includes the three orbitals necessary to describe bond breaking and bond formation and the three electrons in these orbitals. Note that this active space involves molecular orbitals of different type for the reaction channels 1a and 1b and can only be used for separate studies of these channels, whereas the (CO:11/11) active space will provide a smooth potential energy surface in a wider region that involves both reaction channels. The AP scheme builds the active space by enumerating the electrons and orbitals in the fragment atoms. The choice considered in the present work is the full valence active space (AP:15/11); this active space is related to the (CO:11/11) active space by replacing a pair of 3p(O) orbitals by the pair of the 2s(O) orbitals, so it has the same number of active orbitals, but two of them are of different character. The NO scheme is based on the occupation pattern of the natural orbitals generated from the first-order density matrix;[61] this approach has been recently employed, for example, in a study of a closely related hydrogen transfer reaction between two peroxyl radicals.[62] An active space generated in this way will usually be geometry-dependent, whereas for full dynamics calculations, one needs a single set of active orbitals that smoothly change their character across the potential energy surface on the way from reactants to products. Therefore, we did not employ the NO scheme in this work. The CO active space that we employ always includes the σ and σ* orbital pairs for all bonds that are being broken or formed in a particular reaction because these orbital pairs generate the valence bond configurations that participate in the formation of a barrier,[63]

and therefore we regard the CO scheme as the preferred one, but we will also present some results by the AP scheme for comparison.

First, multireference second-order perturbation theory (MRMP2)[64−67] calculations were performed using GAMESS.[68] All orbitals except the 1s(O) were included in the dynamic correlation treatment in the MRMP2 calculations. Second, a few calculations were performed with multireference coupled-cluster theory, in particular with the multireference averaged quadratic coupled cluster (MR-AQCC) method[69] using the COLUMBUS[70] program system. These calculations involve single and double excitations from the active space and may also be called MR-AQCCSD. The one-electron basis sets used for MRCMs in tables are MG3S,[71] which is equivalent to the 6-311+G(2df,-2p)[72] basis if one considers only H and O, aug-cc-pVXZ[73,74] (X = D (double-ζ), X = T (triple-ζ), X = Q (quadruple-ζ)), d-aug-cc-pVTZ,[75] and the augmented triple-ζ atomic natural basis set of Widmark, Malmqvist, and Roos,[76] which will be denoted ANO. The MG3 basis set is also used; it is like MG3S but with 311+ replaced by 311++. We also use the 6-31+G(d,p) basis, sometimes called DIDZ.

Even though the single-reference benchmark methods provide an accurate description of the system in the asymptotic regions, the validity of these methods is questionable in the region of the saddle point for reaction 1a where the reference UHF wavefunctions are severely spin contaminated ($\langle S^2 \rangle \approx 1.0$) (for reaction 1b, $\langle S^2 \rangle$ is ~0.80, which is much closer to the correct value of 0.75). For more reliable transition state geometries and energetics, we have performed full geometry optimization of the reactants and the transition structures at the MRMP2 level with a variety of basis sets. We used a parallel direct determinant implementation of the MRMP2 method available in GAMESS, and numeric gradients. To the best of our knowledge, this is the first study that reports consistently optimized geometries of saddle points and equilibrium structures at the MRMP2 level. We use the term *consistently optimized* to indicate that all relevant stationary points are fully optimized at the same computational level, whereas in some other cases, denoted as A//B, the geometries of reactants, transition states, and/or products are optimized with level B, followed by calculations of the energies at those geometries with a higher-level method. In addition, several structures were consistently optimized at the MR-AQCC level using the analytic gradient method[77] available in the COLUMBUS program system. These calculations also appear to be methodological firsts, and they are discussed in section 3.6.

The hybrid density functionals that are used in the present work include MPW1K,[78] BB1K,[79] MPW1B95,[80] PBE1KCIS,[81] PWB6K,[82] PW6B95,[82] M05,[83] and M05-2X,[84] and PBEKCISX. (PBEKCISX denotes X% Hartree−Fock exchange, $(100−X)$% PBE exchange, and 100% KCIS correlation.) HDFT calculations were spin-unrestricted and carried out using the *Gaussian 03* package[35] and the *MN-GFM* module.[85]

3. Results

3.1. Energies of Reaction, Barrier Heights, and Bond Dissociation Energies. Tables 1 and 2 list the experimental and theoretical single-reference calculations of the energy of each reaction (ΔE), the forward and reverse barrier height of each reaction, and the bond dissociation energies D_e of the breaking bonds, and they also list some experimental values for comparison. Many of the benchmark-level SRML methods are in excellent agreement with experiment for the energy of reaction and the bond dissociation energies. Table 3 presents the forward

Reactions of H Atom with Hydrogen Peroxide

J. Phys. Chem. A, Vol. 111, No. 51, 2007 **13557**

TABLE 1: Zero-Point Exclusive Energies of Reaction, Barrier Heights, and Bond Dissociation Energies for Reaction 1a (in kcal/mol)

method	ΔE	V_f	V_r	D_e(HO−H)	D_e(HO−OH)
benchmark level SRML methods					
BMC-CCSD//MC-QCISD/3	−71.9	5.5	77.4	127.9	56.1
G3SX(MP3)//MC-QCISD/3	−71.4	7.1	78.5	126.4	55.0
G3SX//MC-QCISD/3	−71.1	6.9	78.0	126.3	55.2
G3X//MC-QCISD/3	−71.7	6.8	78.5	124.8	53.1
G3//MC-QCISD/3	−71.6	6.9	78.5	124.6	53.0
G2//MC-QCISD/3	−70.6	7.6	78.1	125.9	55.3
MCG3/3//MC-QCISD/3	−71.7	6.3	78.0	126.9	55.2
CBS-APNO//MC-QCISD/3	−70.7	5.9	76.6	125.8	55.1
CBS-Q//MC-QCISD/3	−70.3	5.7	76.0	125.9	55.7
CBS-QB3//MC-QCISD/3	−70.2	6.0	76.2	125.9	55.8
mean of benchmarks	−71.1	6.5	77.6	126.0	55.0
std dev of benchmarks	0.6	0.7	1.0	1.0	1.1
midlevel MCCMs					
MC3BB	−70.2	10.5	80.8	124.5	54.3
MC3MPW	−70.5	10.5	81.1	123.0	52.5
MC-QCISD/3	−72.2	8.3	80.6	127.9	55.7
MC-QCISD-MPWB	−72.4	7.0	79.4	126.7	54.3
HDFT[a]					
M05-2X/6-31+G(d,p)	−72.5	10.4	82.9	123.1	50.6
M05/MG3S	−74.0	9.5	83.5	124.3	50.3
M05/6-31+G(d,p)	−75.0	8.9	83.8	125.0	50.0
PW6B95/MG3S	−70.4	5.5	75.9	123.3	52.8
PW6B95/6-31+G(d,p)	−70.9	4.9	75.7	123.1	52.2
PWB6K/MG3S	−73.5	8.6	82.1	121.4	47.9
PWB6K/6-31+G(d,p)	−74.3	7.9	82.2	121.2	46.9
BB1K/MG3S	−73.1	8.4	81.5	122.1	49.0
BB1K/6-31+G(d,p)	−73.8	7.8	81.6	121.8	48.0
MPW1K/MG3S	−74.9	7.8	82.6	118.9	44.0
MPW1K/6-31+G(d,p)	−75.5	7.2	82.7	118.7	43.2
MPW1B95/MG3	−69.8	6.2	75.9	123.6	53.9
MPW1B95/MG3S	−69.8	6.3	76.1	123.7	53.9
MPW1B95/6-31+G(d,p)	−70.4	5.7	76.1	123.5	53.1
experimental values[b]	−71.2			125.1	53.9

[a] Spin-unrestricted. [b] Values for ΔE, D_e(HO−H), and D_e(HO−OH) were determined as explained in section 2.2.

barrier heights determined by MRMP2 calculations, and Table 4 compares MR-AQCC and CCSD(T) forward barrier heights. All quantities in Tables 1−4 are zero-point exclusive. Tables 5 and 6 list the theoretical geometries of each saddle point; the unscaled harmonic vibrational frequencies calculated for these structures are listed in Tables S7 and S8 of the Supporting Information. Figures 1 and 2 define the internal coordinates that are used in Tables 5 and 6 and in the CVT/SCT calculations. The theoretical and experimental geometries and unscaled harmonic frequencies of each reactant and product are tabulated in the Supporting Information.

From Tables 1 and 2 we calculate that the energies of reaction predicted by the benchmark-level methods have mean unsigned errors of 0.5 and 0.2 kcal/mol, respectively, where the unsigned error is an absolute value of the difference between the calculated and experimental energy of reaction, and the maximum unsigned errors are 1.0 and 0.7 kcal/mol, respectively. The average forward barrier heights of reaction 1a and reaction 1b that were calculated by the benchmark-level MCCM methods are 6.5 and 9.9 kcal/mol, and they have standard deviations of 0.7 and 0.4 kcal/mol.

3.2. Diagnostics for Multireference Character. Two types of diagnostics have been to employed to test for the multireference character of reactions 1a and 1b: the B_1[86,87] diagnostic that applies to a particular chemical bond and the T_1[88] diagnostic that refers to a molecular system.

The B_1 diagnostic involves calculating a bond energy at the BLYP[89,90] and B1LYP//BLYP levels of theory, where B1LYP//BLYP is defined as a B1LYP[91] single-point energy at the BLYP geometry. The B_1 diagnostic is defined as the magnitude of the

difference in these bond energies divided by the number of bonds being broken and then divided by 1 kcal/mol to make the diagnostic unitless; this difference in bond energies tends to be larger when multireference character is present in the bond because density functional GGAa include some static correlation in the exchange functional but Hartree−Fock exchange does not account for static correlation. In this Article we apply this diagnostic to the breaking bond of each reaction. The bond energies and B_1 diagnostics for reactions 1a and 1b are listed in Table 7. A value of 10 is the recommended borderline at which (if $B_1 > 10$) the bond should be considered a multireference case.[86,87] The value of 10.64 for reaction 1a exceeds the nominal single-reference limit, whereas the value of 0.13 for reaction 1b is well below it.

The next diagnostic involves examining the difference between a CCSD(T)[92−95] single-point energy calculation with Kohn−Sham orbitals[96] as the reference and one with and Hartree−Fock (HF) orbitals[97] as the reference.[87,98] The Kohn−Sham orbitals are calculated using the BLYP method, and the single-point energy calculation is done at the UCCSD(T) level of theory with the aug-cc-pVTZ basis set. The coupled-cluster calculations with Kohn−Sham orbitals were carried out using MOLPRO.[99] The differences in energy between the UCCSD-(T)/aug-cc-pVTZ single-point energies with Kohn−Sham and Hatree−Fock orbitals are tabulated in Table 8. Additionally, the T_1 diagnostic (as calculated by MOLPRO) is listed in Table 8 for each species and set of reference orbitals. The T_1 diagnostic is a normalized measure of the contribution of all single excitations to the post-Hartree−Fock wave function, calculated as described elsewhere.[88] The recommended[88] value of the T_1

TABLE 2: Zero-Point Exclusive Energies of Reaction, Barrier Heights, and Bond Dissociation Energies for Reaction 1b (in kcal/mol)

method	ΔE	V_f	V_r	$D_e(H-H)$	$D_e(HOO-H)$
benchmark level SRML methods					
BMC-CCSD//MC-QCISD/3	−16.3	10.1	26.4	110.7	94.3
G3SX(MP3)//MC-QCISD/3	−15.8	10.1	25.9	109.9	94.1
G3SX//MC-QCISD/3	−15.7	9.9	25.6	109.8	94.2
G3X//MC-QCISD/3	−16.5	9.9	26.4	110.0	93.5
G3//MC-QCISD/3	−16.4	10.0	26.4	109.7	93.3
G2//MC-QCISD/3	−16.0	10.4	26.4	110.3	94.3
MCG3/3//MC-QCISD/3	−16.6	9.7	26.3	110.9	94.2
CBS-APNO//MC-QCISD/3	−16.3	9.0	25.3	109.9	93.5
CBS-Q//MC-QCISD/3	−16.2	10.4	26.6	110.5	94.3
CBS-QB3//MC-QCISD/3	−16.4	9.5	25.9	110.7	94.3
mean of benchmarks	−16.2	9.9	26.1	110.2	94.0
std dev of benchmarks	0.3	0.4	0.4	0.4	0.4
midlevel MCCMs					
MC3BB	−15.7	9.1	24.8	107.2	91.5
MC3MPW	−14.1	9.2	23.4	105.5	91.3
MC-QCISD/3	−16.2	10.3	26.5	111.2	95.0
MC-QCISD-MPWB	−17.2	8.4	25.7	110.1	92.9
HDFT[a]					
M06-2X/MG3S	−16.3	8.9	25.0	108.3	92.0
M05-2X/MG3S	−16.3	9.5	25.8	107.5	91.2
M05-2X/6-31+G(d,p)	−17.1	8.8	25.9	107.9	90.7
M05/MG3S	−19.4	6.8	26.2	108.7	89.3
M05/6-31+G(d,p)	−20.7	6.1	26.8	111.0	90.3
PW6B95/MG3S	−19.3	5.0	24.3	108.3	89.0
PW6B95/6-31+G(d,p)	−20.3	4.4	24.8	109.8	89.5
PWB6K/MG3S	−17.7	8.5	26.2	106.4	88.7
PWB6K/6-31+G(d,p)	−18.6	8.0	26.6	107.9	89.3
BB1K/MG3S	−18.6	7.9	26.5	107.3	88.7
BB1K/6-31+G(d,p)	−19.5	7.4	27.0	108.6	89.1
MPW1K/MG3S	−17.8	7.5	25.3	104.9	87.1
MPW1K/6-31+G(d,p)	−18.4	7.3	25.7	106.2	87.8
MPW1B95/MG3S	−18.3	5.7	24.0	107.3	89.0
MPW1B95/6-31+G(d,p)	−19.4	5.1	24.5	108.9	89.5
experimental values[b]	−16.4			109.6	93.1

[a] Spin-unrestricted. [b] Values for ΔE, $D_e(H-H)$, and $D_e(HOO-H)$ were determined as explained in section 2.2.

TABLE 3: Forward Barrier Heights for Reactions 1a and 1b (in kcal/mol) Calculated at the MRMP2 Level

method	V_{f1a}	V_{f1b}
at consistently optimized geometries		
MRMP2(CO:11/11)/ANO	4.8	9.2
MRMP2(CO:3/3)/ANO	4.8	
MRMP2(CO:11/11)/d-aug-cc-pVTZ	4.9	8.9
MRMP2(CO:3/3)/d-aug-cc-pVTZ	4.9	
MRMP2(AP:15/11)/aug-cc-pVTZ	4.6	
MRMP2(CO:11/11)/aug-cc-pVTZ	4.8	9.0
MRMP2(CO:3/3)/aug-cc-pVTZ	4.9	
MRMP2(CO:11/11)/aug-cc-pVDZ	4.8	9.9
MRMP2(CO:11/11)/MG3S	6.0	10.0
MRMP2(CO:3/3)/MG3S	6.0	8.9
at MRMP2(CO:11/11)/aug-cc-pVTZ geometries		
MRMP2(AP:15/11)/aug-cc-pVQZ	4.8	
MRMP2(CO:11/11)/aug-cc-pVQZ	5.0	9.1

TABLE 4: Forward Barrier Heights for Reactions 1a and 1b (in kcal/mol) Calculated at MR-AQCC and CCSD(T)// MR-AQCC Levels

method	V_{f1a}	V_{f1b}
at consistently optimized geometries		
MR-AQCC(CO:3/3)/MG3S	7.3	10.4
MR-AQCC(CO:3/3)/aug-cc-pVDZ	5.5	9.2
at MR-AQCC(CO:3/3)/MG3S geometries		
KS-UCCSD(T)/aug-cc-pVQZ[a]	6.1	9.7
RHF-UCCSD(T)/aug-cc-pVQZ	6.1	9.7
KS-UCCSD(T)/aug-cc-pVTZ[a]	5.9	9.4
RHF-UCCSD(T)/aug-cc-pVTZ	6.0	9.4
UHF-CCSD(T)/aug-cc-pVTZ	6.3	9.5
UHF-CCSD(T)/MG3S	7.5	10.5
UHF-CCSD(T)/aug-cc-pVDZ	5.8	9.9

[a] The Kohn−Sham orbitals used for these coupled cluster calculations are spin-restricted and are based on the BLYP density functional.

diagnostic at which a system should be considered to be a multireference case (such that single-reference calculations are potentially unreliable) is $T_1 > 0.02$.

The HOOH, HOO, and the two transition state structures show considerable multireference character. Each species with an O−O double-bond has at least a 1.0 kcal/mol difference between the UCCSD(T) energies with the different reference orbitals. Also, several species, including both transition states with both sets of orbitals, surpass the 0.02 criterion for the T_1 diagnostic. These diagnostics certainly bring the validity of the single-reference electronic structure methods into question. The barrier heights and energies of reactions 1a and 1b as calculated by the methods used to generate orbitals for the UCCSD(T) calculations are listed in Table 9. Despite the fact that a change

in reference orbitals can change the UCCSD(T)/aug-cc-pVTZ energy by about 1 kcal/mol, it is shown that reference calculations themselves yield similar results. The difference in energy is at worst 0.11 kcal/mol in the reaction energy and 0.07 kcal/mol in the barrier height.

The results from the diagnostics help to explain the large disparity between the methods listed in Tables 1 and 2. (Such a disparity was not unexpected because of the well-known near degeneracy effects in the electronic structure of the O−O bond). The forward barrier height for reaction 1a ranges from 5.5 to 7.6 kcal/mol in the benchmark-type single-reference calculations and from 4.9 to 11.0 kcal/mol in the DFT calculations. Clearly, reaction 1a has multireference character, although the diagnostics

Reactions of H Atom with Hydrogen Peroxide

J. Phys. Chem. A, Vol. 111, No. 51, 2007 **13559**

TABLE 5: Optimized Geometries for the Saddle Point of Reaction 1a (Bond Lengths in Å, Bond Angles and Torsion Angles in Degrees)

method	R_1	R_2	R_3	R_4	A_1	A_2	A_3	A_4	τ_1
HDFT[a]									
M05-2X/MG3S	0.962	1.506	0.964	1.576	99.3	99.5	94.0	166.5	117.8
M05-2X/6-31+G(d,p)	0.966	1.511	0.968	1.595	98.8	99.2	95.4	165.1	123.8
M05/MG3S	0.963	1.514	0.965	1.590	99.3	99.3	95.1	165.5	117.2
M05/6-31+G(d,p)	0.968	1.520	0.970	1.612	98.9	98.9	95.9	164.8	121.4
PW6B95/MG3S	0.961	1.519	0.962	1.613	98.8	99.0	94.3	166.7	118.3
PW6B95/6-31+G(d,p)	0.966	1.525	0.967	1.634	98.4	98.6	95.6	165.5	123.4
PWB6K/MG3S	0.954	1.512	0.955	1.544	99.1	99.0	93.8	167.2	118.9
PWB6K/6-31+G(d,p)	0.958	1.518	0.960	1.564	98.7	98.6	95.2	166.2	123.9
BB1K/MG3S	0.956	1.510	0.957	1.551	99.1	99.1	94.0	166.9	118.3
BB1K/6-31+G(d,p)	0.960	1.516	0.962	1.571	98.7	98.7	95.4	165.8	123.4
MPW1K/MG3S	0.955	1.504	0.956	1.551	99.3	99.3	93.6	167.0	117.8
MPW1K/6-31+G(d,p)	0.959	1.510	0.960	1.570	98.9	98.9	95.2	165.8	123.2
MPW1B95/MG3	0.961	1.512	0.962	1.588	99.0	99.2	94.7	166.1	117.8
MPW1B95/MG3S	0.961	1.513	0.962	1.589	98.9	99.1	94.3	166.6	117.8
MPW1B95/6-31+G(d,p)	0.965	1.519	0.966	1.610	98.5	98.7	95.7	165.3	122.9
midlevel MCCMs									
MC3BB	0.961	1.499	0.963	1.486	99.5	99.7	95.6	164.6	116.9
MC3MPW	0.962	1.493	0.964	1.470	99.7	100.0	95.7	164.1	116.3
MC-QCISD/3	0.968	1.536	0.969	1.560	98.1	98.2	92.9	168.8	116.9
MC-QCISD-MPWB	0.964	1.532	0.965	1.582	98.3	98.4	93.0	168.6	116.8
MRCMs[b]									
MRMP2(11/11)/(ANO)	0.969	1.570	0.970	1.671	96.5	96.5	92.7	168.5	117.2
MRMP2(3/3)/(ANO)	0.965	1.565	0.966	1.651	96.7	96.6	91.3	172.1	120.6
MRMP2(11/11)/*d*-aug-cc-pVTZ[c]	0.972	1.577	0.973	1.665	96.3	96.2	61.4	170.3	116.5
MRMP2(3/3)/*d*-aug-cc-pVTZ[c]	0.969	1.568	0.970	1.652	96.6	96.5	91.1	172.3	120.0
MRMP2(AP:15/11)/aug-cc-pVTZ	0.971	1.564	0.972	1.658	97.0	97.2	92.9	169.7	118.6
MRMP2(11/11)/aug-cc-pVTZ	0.973	1.575	0.974	1.670	96.4	96.4	92.5	169.1	115.9
MRMP2(3/3)/aug-cc-pVTZ	0.968	1.568	0.970	1.653	96.6	96.6	91.2	172.1	120.0
MRMP2(11/11)/MG3S	0.970	1.581	0.971	1.650	96.2	96.1	91.3	169.5	121.1
MR-AQCC(3/3)/MG3S	0.963	1.565	0.964	1.590	97.3	97.2	92.7	167.1	119.4
MR-AQCC(3/3)/aug-cc-pVDZ	0.971	1.580	0.973	1.651	97.2	96.8	92.7	163.0	114.0
MR-AQCC(3/3)/*d*-aug-cc-pVDZ[c]	0.971	1.579	0.972	1.649	97.3	97.0	92.4	162.9	113.3

[a] Spin-unrestricted. [b] The CO scheme is used for the active space, unless otherwise indicated; see section 2.3. [c] Double set of diffuse functions on oxygen, and single set of diffuse functions on all hydrogen atoms.

TABLE 6: Optimized Geometries for the Saddle Point of Reaction 1b (Bond Lengths in Å, Bond Angles and Torsion Angles in Degrees)

method	R_1	R_2	R_3	R_4	A_1	A_2	A_H	τ_1	τ_2
HDFT[a]									
M06-2X/MG3S	0.965	1.379	1.125	0.990	103.4	105.3	175.4	98.0	96.0
M05-2X/MG3S	0.963	1.382	1.114	1.007	103.2	105.2	175.5	99.0	96.9
M05-2X/6-31+G(d,p)	0.967	1.390	1.109	1.021	102.9	105.0	174.7	101.4	98.8
M05/MG3S	0.966	1.374	1.069	1.102	103.4	106.0	174.4	100.5	97.7
M05/6-31+G(d,p)	0.970	1.382	1.066	1.120	103.1	105.6	172.9	103.0	99.5
PW6B95/MG3S	0.963	1.390	1.092	1.041	102.8	105.4	175.1	99.6	97.2
PW6B95/6-31+G(d,p)	0.967	1.400	1.088	1.055	102.5	105.0	174.5	102.1	99.4
PWB6K/MG3S	0.955	1.364	1.112	0.990	103.7	105.8	175.7	98.0	96.0
PWB6K/6-31+G(d,p)	0.959	1.374	1.111	0.997	103.3	105.5	175.5	100.1	98.0
BB1K/MG3S	0.957	1.367	1.108	1.002	103.5	105.8	175.8	98.2	96.1
BB1K/6-31+G(d,p)	0.961	1.376	1.106	1.011	103.2	105.5	175.4	100.4	98.2
MPW1K/MG3S	0.956	1.364	1.111	0.992	103.7	105.8	175.7	97.7	95.8
MPW1K/6-31+G(d,p)	0.960	1.373	1.108	0.999	103.4	105.5	175.7	100.0	97.9
MPW1B95/MG3S	0.962	1.380	1.099	1.030	103.1	105.6	175.3	99.0	96.7
MPW1B95/6-31+G(d,p)	0.966	1.390	1.095	1.042	102.8	105.3	174.7	101.5	98.9
midlevel MCCMs									
MC3BB	0.963	1.378	1.141	0.959	103.1	105.9	175.8	97.9	96.0
MC3MPW	0.964	1.379	1.152	0.942	103.1	106.0	175.7	97.6	95.6
MC-QCISD/3	0.969	1.407	1.163	0.947	101.9	104.5	175.6	97.9	95.9
MC-QCISD-MPWB	0.965	1.392	1.141	0.971	102.5	105.1	175.5	97.9	95.8
MRCMs[b]									
MRMP2(11/11)/*d*-aug-cc-pVTZ[c]	0.973	1.443	1.128	1.005	100.2	102.9	173.9	97.4	94.5
MRMP2(11/11)/aug-cc-pVTZ	0.972	1.443	1.128	1.005	100.2	102.9	173.7	97.6	94.6
MRMP2(11/11)/MG3S	0.971	1.436	1.129	1.001	100.5	103.1	173.5	99.1	96.0
MRAQCC(3/3)/MG3S	0.963	1.404	1.144	0.973	102.0	104.7	174.8	99.7	97.3
MRAQCC(3/3)/aug-cc-pVDZ	0.971	1.430	1.147	0.996	101.0	104.2	171.8	102.7	98.8

[a] Spin-unrestricted. [b] The CO scheme is used for the active space; see section 2.3. [c] Double set of diffuse functions on oxygen, and single set of diffuse functions on all hydrogen atoms.

show that the higher-level methods are able to compensate for this to some extent, which is why various SRML benchmark calculations agree within ~2 kcal/mol. Reaction 1b also has some multireference character, but the B_1 diagnostic (discussed

TABLE 7: Bond Energies (kcal/mol) and B_1 Diagnostic (See Text)

	BLYP	B1LYP	B_1 diagnostic
1a (O−O energy)	56.74	46.10	10.64
1b (H−O energy)	87.47	87.60	0.13

TABLE 8: T_1 Diagnostic Based on UCCSD(T)/aug-cc-pVTZ with RHF[a] and BLYP[b] Orbitals and Differences in Energy

molecule	E(BLYP) − E(HF) (kcal/mol)	T_1 (HF)	T_1 (BLYP)
HOOH	1.16	0.013	0.013
H	0.00	0.000	0.023
H_2O	0.56	0.010	0.013
OH	0.595	0.009	0.014
H_2	0.00	0.005	0.015
HOO	1.04	0.038	0.017
1a[c]	1.09	0.025	0.020
1b[c]	1.14	0.024	0.024

[a] RHF for even number of electrons; ROHF for odd number of electrons. [b] RB3LYP and ROB3LYP. [c] Transition state geometries.

TABLE 9: Barrier Heights and Energies of Reaction for UCCSD(T)/aug-cc-pVTZ with HF and BLYP Orbitals (kcal/mol)

	HF	BLYP	BLYP-HF
V_{f1a}	6.13	6.06	−0.07
ΔE_{1a}	−71.38	−71.39	0.00
V_{f1b}	9.38	9.36	−0.02
ΔE_{1b}	−15.82	−15.93	−0.11

TABLE 10: Rate Coeffiicients (cm^3 $molecule^{-1}$ s^{-1}) from Experimental Publications

source	reaction	T (K)	k
Gorse−Volman	1a	298	5.7E-15
Gorse−Volman	1b	298	3.1E-15
Albers *et al.*	1a	294	5.16E-15
		297	5.16E-15
		299	4.73E-15
		328	9.46E-15
		358	1.59E-14
		389	2.49E-14
		422	3.57E-14
		464	6.58 E-14
Baldwin *et al.*	1b	713	1.2 E-12[a]
		743	1.3E-12
		753	1.4E-12[a]
		773	1.9E-12[a]
Klemm *et al.*.	1a + 1b	283	3.14E-14[a]
		298	5.24E-14[a]
		299	5.29E-14[a]
		300	5.30E-14[a]
		301	5.58E-14[a]
		333	6.70E-14[a]
		353	1.01E-13[a]
Michael *et al.*	1a + 1b	298	(4.50 ± 0.20)E-14
		359	(9.90 ± 0.47)E-14

[a] In these cases there was more than one measurement at a given T, and we averaged them with equal weights.

above) indicates that it is not as large as in reaction 1a, which explains why the HDFT methods do not differ as much from each other as they do for reaction 1a.

3.3. Rate Coefficient Calculations for Reaction 1a. As a first approach to studying reaction 1a, CVT/SCT rate coefficients were calculated for a range of barrier heights and compared to the published experimental results. Table 10 lists the published experimental rate coefficients[7−18] that will be considered. It was determined that the barrier heights calculated by the PBEKCIS*X* functionals smoothly increase for reaction 1a as the percentage of Hartree−Fock exchange is increased. Table 11 shows the

TABLE 11: Barrier Heights and Energies of Reaction (kcal/mol) for Reaction 1a with PBEKCIS*X*/MG3

percent HF exchange (X)	V_f	ΔE
20	3.3	−70.3
25	4.1	−71.7
30	4.9	−73.1
35	5.6	−74.4
40	6.4	−75.7
45	7.2	−76.9

barrier heights and energies of reaction for 1a with PBEKCIS*X*/MG3, as X ranges from 20 to 45%.

A frequency scaling factor of 0.9833 was determined for the PBE1KCIS[81]/MG3 level of theory using the method of Fast *et al.*[100] Using the PBEKCIS*X* naming convention, the PBE1KCIS method is equivalent to PBEKCIS22. A more complete procedure would be to optimize the scaling factor for each value of X; however, applying the same scaling factor for all values of X is adequate here because the expected difference in the results due to re-optimizing this factor are smaller than other uncertainties in the calculations.

The rate coefficients for a large number of temperatures are listed in Supporting Information and are plotted in Figure 3. Figure 3 also contains experimental values. The rate coefficients for reaction 1a have been determined at room temperature by Gorse and Volman[16,17] and at high temperature by Baldwin *et al.*[7−14] Also, the values for k_1 have been determined by Klemm *et al.*[18a] and Michael *et al.*[18b] at low temperatures and by Albers
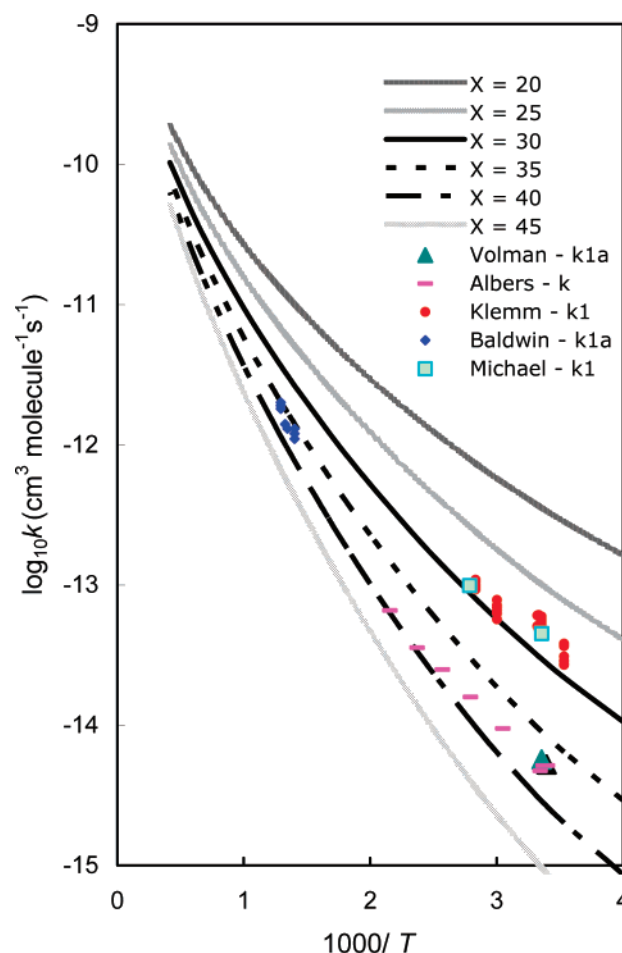
Figure 3. (1a) CVT/SCT rate coefficients with the Cω scheme for the torsional mode using PBEKCIS*X*, where X represents the amount of HF exchange, plotted with experimentally determined recommended values for the rate coefficients.

Reactions of H Atom with Hydrogen Peroxide

J. Phys. Chem. A, Vol. 111, No. 51, 2007 **13561**

TABLE 12: CVT/SCT Rate Coefficients (cm³ molecule⁻¹ s⁻¹) for Reaction 1a Using MPW1B95/MG3

T (K)	CVT/SCT(harmonic)	CVT/SCT (Cω)^a
250	9.90E-16	9.89E-16
283	2.53E-15	2.53E-15
298	3.75E-15	3.75E-15
300	3.95E-15	3.95E-15
301	4.05E-15	4.05E-15
333	8.71E-15	8.70E-15
353	1.34E-14	1.34E-14
350	1.26E-14	1.26E-14
400	3.30E-14	3.29E-14
450	7.36E-14	7.35E-14
500	1.45E-13	1.45E-13
550	2.59E-13	2.58E-13
600	4.28E-13	4.26E-13
700	9.79E-13	9.73E-13
713	1.07E-12	1.07E-12
743	1.32E-12	1.31E-12
753	1.41E-12	1.40E-12
773	1.60E-12	1.59E-12
800	1.89E-12	1.87E-12
1000	5.03E-12	4.97E-12
1500	2.19E-11	2.15E-11
2400	8.18E-11	7.95E-11

^{a} Cω denotes that the torsion is treated by the Cω scheme of ref 89, and all other modes are treated in the harmonic approximation.

et al.[15] at medium temperatures. These values for k_1 have been plotted in Figure 3 because some of the authors determined[15,18] that reaction 1a dominated the rate coefficient at low temperatures.

Figure 3 prompts two important observations. The first is that the rate coefficients determined by Klemm *et al.*[18a] and Michael *et al.*[18b] in the same laboratory do not agree with the other experimentally determined rate coefficients. The second observation is that the PBEKCIS*X* curves indicate that, if the results of Volman, Baldwin, and Albers are reliable, then the barrier height for reaction 1a is approximately 6.4 kcal/mol, which is the value of the barrier height for PBEKCIS40. On the other hand, if the results by Klemm *et al.* are reliable, then the barrier height for reaction 1a is approximately 4.6 kcal/mol; this corresponds to the barrier height between PBEKCIS25 and PBEKCIS30.

Although the barrier height of PBEKCIS40 appears to approximately correspond to the data by Gorse and Volman,[16,17] Baldwin *et al.*,[7–14] and Albers *et al.*,[15] the reaction energy of −75.7 kcal/mol is significantly in error. Therefore, we will now choose an electronic structure method that has a barrier height that yields rate constants like their experimental ones and also yields a reaction energy closer to the experimental value of −71.17 kcal/mol. The MPW1B95/MG3 level of theory is chosen because it yields a barrier height of 6.2 kcal/mol and an energy of reaction of −69.8 kcal/mol. The MG3 basis set was chosen over the MG3S basis set because it is slightly larger; however, Table 1 shows that the difference in the prediction of these two basis sets is negligible.

The CVT/SCT rate coefficients for reaction 1a as calculated by the MPW1B95/MG3 method are listed in Table 12 and plotted in Figure 4. The frequencies along the minimum energy path (MEP) are plotted in Figure 5. The potential energy along the MEP, $V_{MEP}(s)$, and the vibrationally adiabatic ground state energy (or zero-point-inclusive potential energy), $\Delta V_a^G(s)$, are plotted in Figure 6. (Note that $V_{MEP}(s)$ and $\Delta V_a^G(s)$ are each relative to their value at reactants, taken as the zero of energy.) Rate coefficients calculated with a harmonic torsion are also listed in Table 12. A comparison of these rate coefficients to
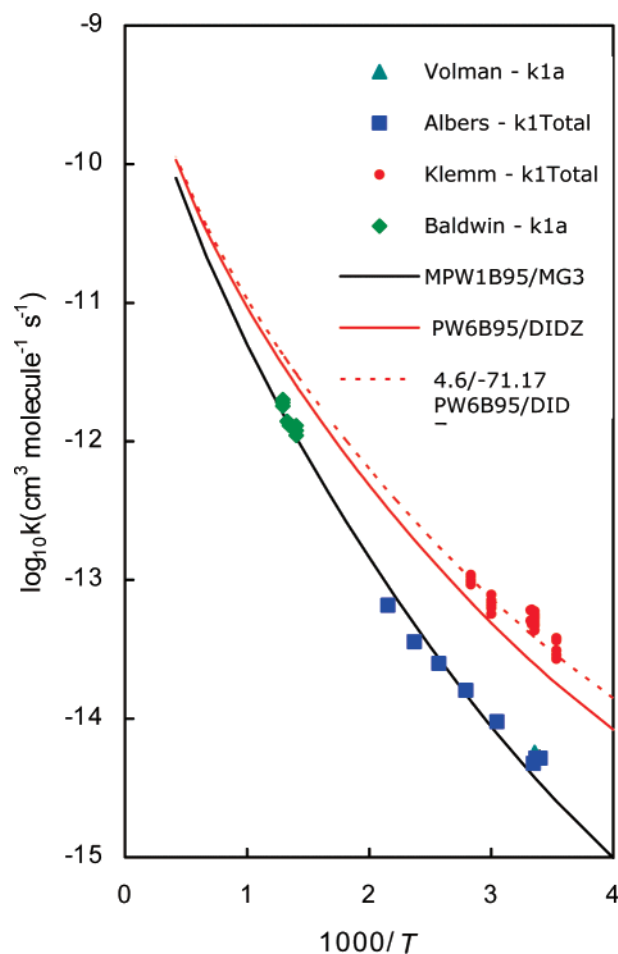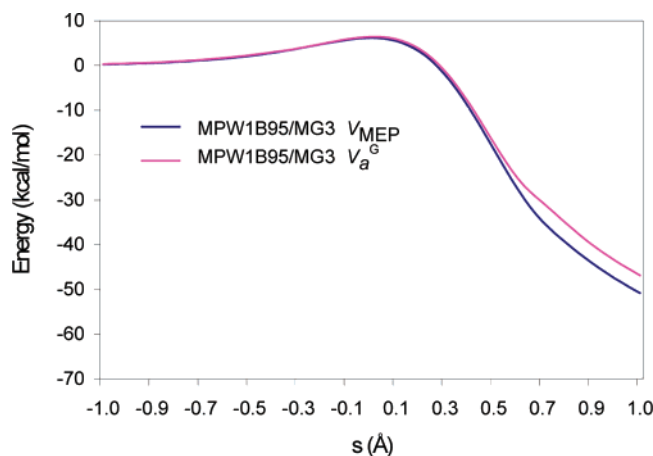

Figure 4. (1a) CVT/SCT rate coefficients with the Cω scheme for the torsional mode using MPWB195/MG3, PW6B95/DIDZ, and 4.6/−71.17 PW6B95/DIDZ, plotted with experimental determined recommended values for the rate coefficients.
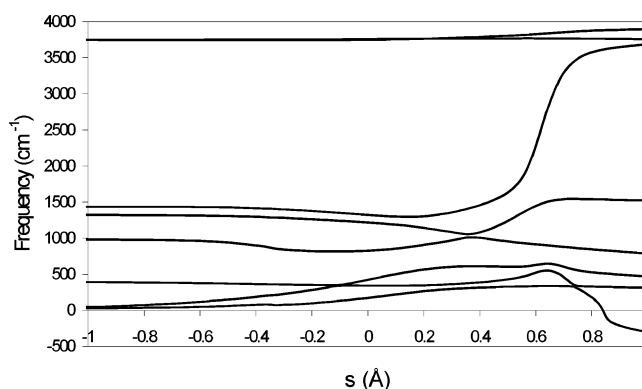
Figure 5. Frequencies calculated with MPWB195/MG3 for reaction 1a as functions of the reaction coordinate s, which is the signed distance along the reaction path from the saddle point. These frequencies are based on the RODS scheme with redundant internal coordinates.

the unharmonic ones for the same potential energy surface shows that the torsional motion is largely harmonic for this reaction. Previous research[38a] indicates that H_2O_2 is adequately represented for all but the highest temperatures by a multiconformer harmonic oscillator model, where the two degenerate wells are both counted. The transition state also has two degenerate wells, which allows for the simple harmonic oscillator to result in a fortuitous cancellation of error. However, small torsional effects occur as the temperature increases, so all finalized and plotted calculations include the Cω scheme for the torsional motion of

Figure 6. $V_{MEP}(s)$ and $\Delta V_a^G(s)$ with MPWB195/MG3 for reaction 1a as functions of the reaction coordinate s, which is the signed distance along the reaction path from the saddle point.

TABLE 13: CVT/SCT Rate Coefficients (cm³ molecule⁻¹ s⁻¹) for Reaction 1a Using the 4.6/−71.17 Calculation

T (K)	CVT/SCT(harmonic)	CVT/SCT (Cω)[a]
250	1.40E-14	1.40E-14
283	2.87E-14	2.87E-14
298	3.87E-14	3.87E-14
300	4.03E-14	4.02E-14
301	4.10E-14	4.10E-14
333	7.34E-14	7.34E-14
353	1.02E-13	1.02E-13
350	9.74E-14	9.73E-14
400	2.03E-13	2.03E-13
450	3.77E-13	3.77E-13
500	6.38E-13	6.37E-13
550	1.00E-12	1.00E-12
600	1.49E-12	1.49E-12
700	2.88E-12	2.86E-12
713	3.10E-12	3.08E-12
743	3.65E-12	3.63E-12
753	3.85E-12	3.83E-12
773	4.27E-12	4.24E-12
800	4.87E-12	4.84E-12
1000	1.08E-11	1.07E-11
1500	3.69E-11	3.64E-11
2400	1.16E-10	1.14E-10

[a] Cω denotes that the torsion is treated by the Cω scheme of ref 89, and all other modes are treated in the harmonic approximation.

the H_2O_2 reactant and the generalized transition states. The MPW1B95/MG3 rate coefficients are in excellent agreement with the experimentally determined rate coefficients of Gorse and Volman,[16,17] Albers *et al.*,[15] and Baldwin *et al.*[7−14]

Analogously, we have selected the PW6B95/DIDZ method, which yields a barrier height of 4.9 kcal/mol (Table 1), for comparison with the data obtained by Klemm *et al.*[18] The CVT/SCT rate coefficients for reaction 1a as calculated by this method appear to be slightly too small compared to the experimental data, implying that the barrier height should be smaller. To correct for this, a VTST-ISPE calculation was run in which the barrier height was set to 4.6 kcal/mol, and the energy of reaction was set to the best estimate of −71.17 kcal/mol. This calculation is labeled "4.6/−71.17" in Table 13 and Figure 4. The $V_{MEP}(s)$, and $\Delta V_a^G(s)$ curves calculated with this method are plotted in Figure S1 of the Supporting Information. The "4.6/−71.17" rate coefficients agree well with the data by Klemm *et al.*[18]

3.4. Rate Coefficient Calculations for Reaction 1b. The benchmark calculations for reaction 1b indicate that the barrier is large, in the approximately 9.0 to 10.4 kcal/mol range. The

TABLE 14: CVT/SCT Rate Coefficients (cm³ molecule⁻¹ s⁻¹) for Reaction 1b and for the Sum of 1a and 1b

T (K)	1b CVT/SCT (harmonic)[a]	1b CVT/SCT (Cω)[a,b]	1b 10.4/−16.4 (Cω)	1a + 1b set i[c]	1a + 1b set ii[d]
250	1.56E-16	1.56E-16	6.60E-17	1.06E-15	1.42E-14
283	4.81E-16	4.81E-16	2.09E-16	2.74E-15	2.92E-14
298	7.57E-16	7.58E-16	3.33E-16	4.08E-15	3.95E-14
300	8.02E-16	8.03E-16	3.53E-16	4.30E-15	4.10E-14
301	8.26E-16	8.26E-16	3.64E-16	4.41E-15	4.18E-14
333	1.94E-15	1.94E-15	8.82E-16	9.58E-15	7.53E-14
353	3.11E-15	3.12E-15	1.45E-15	1.48E-14	1.05E-13
350	2.91E-15	2.91E-15	1.35E-15	1.39E-14	1.00E-13
400	8.18E-15	8.20E-15	3.98E-15	3.69E-14	2.11E-13
450	1.91E-14	1.92E-14	9.77E-15	8.33E-14	3.96E-13
500	3.90E-14	3.91E-14	2.08E-14	1.66E-13	6.76E-13
550	7.15E-14	7.19E-14	3.97E-14	2.98E-13	1.07E-12
600	1.21E-13	1.22E-13	6.97E-14	4.96E-13	1.61E-12
700	2.88E-13	2.91E-13	1.77E-13	1.15E-12	3.15E-12
713	3.17E-13	3.21E-13	1.97E-13	1.27E-12	3.40E-12
743	3.94E-13	4.00E-13	2.48E-13	1.56E-12	4.03E-12
753	4.23E-13	4.29E-13	2.68E-13	1.67E-12	4.26E-12
773	4.83E-13	4.91E-13	3.09E-13	1.90E-12	4.73E-12
800	5.75E-13	5.84E-13	3.73E-13	2.24E-12	5.42E-12
1000	1.64E-12	1.68E-12	1.16E-12	6.13E-12	1.24E-11
1500	8.12E-12	8.57E-12	6.63E-12	2.81E-11	4.50E-11
2400	2.44E-11	2.69E-11	2.31E-11	1.03E-10	1.41E-10

[a] M05-2X/MG3S. [b] Cω denotes that the torsion is treated by the Cω scheme of ref 89, and all other modes are treated in the harmonic approximation. [c] Estimate based on MPW1B95/MG3 for (1a) from Cω results of Table 12 added to estimate based on 10.4/−16.4(Cω) for (1b) from this table. This is called set i. Estimate based on 4.6/−71.17 data from Table 13 for (1a) and M05-2X/MG3S (Cω) results from this table for (1b). This is called set ii. [d] No ref given.

M05-2X/MG3S level of theory is the only HDFT method with a barrier height in that range, so it has been chosen to study the dynamics for reaction 1b. The M05-2X/MG3S level of theory yields a barrier height of 9.5 kcal/mol and an energy of reaction of −16.3 kcal/mol.

The CVT/SCT rate coefficients for reaction 1b using M05-2X/MG3S are listed in Table 14 and plotted in Figure 7. Once again, the results with a harmonic treatment of torsion have been compared to an anharmonic treatment, and this comparison shows that torsional anharmonicity has only a small effect on the rate coefficient. Along the reaction path in the harmonic calculation, only the generalized normal mode with the second-lowest real frequency is treated with a torsional method; this generalized normal mode primarily corresponds to the spectator H−O group rotating with respect to the O−H−H group. All other generalized normal modes are dominated by bends and stretches. The frequencies for the M05-2X/MG3S method are plotted in Figure 8, and the $V_{MEP}(s)$ and $\Delta V_a^G(s)$ curves are shown in Figure 9. Figure 8 shows that some frequencies are imaginary (plotted as negative) on the reactant side. The spurious imaginary frequencies are far enough from the saddle point that they have no effect on the CVT results and only a very small effect on the tunneling calculations. Indeed, the $V_{MEP}(s)$ and $\Delta V_a^G(s)$ curves shown in Figure 9 are smooth. The maximum of the $\Delta V_a^G(s)$ curve is several kcal/mol lower than the maximum of the $V_{MEP}(s)$ curve.

The M05-2X/MG3S rate coefficients fall between the experimentally determined values of Gorse and Volman[16,17] and Baldwin *et al.*[7−14] The experimental work done by Baldwin *et al.*[7−14] is by far the most extensive and complete. Furthermore, the large rate coefficient recommended by Gorse and Volman for reaction 1b is in disagreement with the conclusions of Klemm *et al.*[18] and Albers *et al.*[15] that k_{1b} does not contribute

Reactions of H Atom with Hydrogen Peroxide

J. Phys. Chem. A, Vol. 111, No. 51, 2007 **13563**
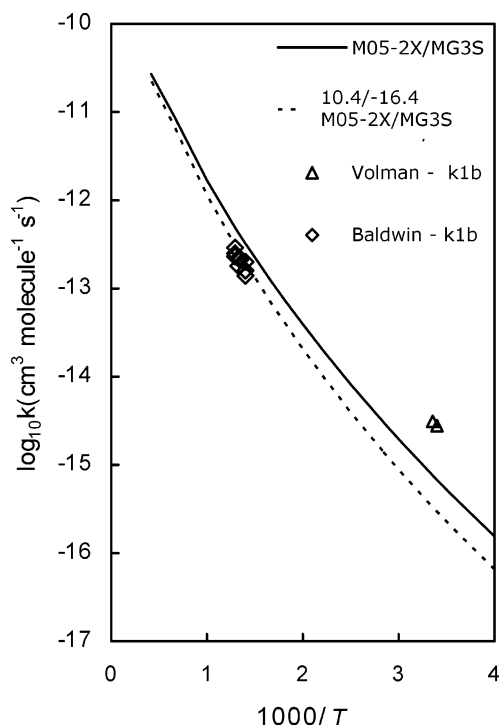
Figure 7. (1b) CVT/SCT rate coefficients with the Cω scheme for the torsional mode using M05-2X/MG3S and 10.4/−16.4 M05-2X/MG3S, plotted with experimental values for the rate coefficients.
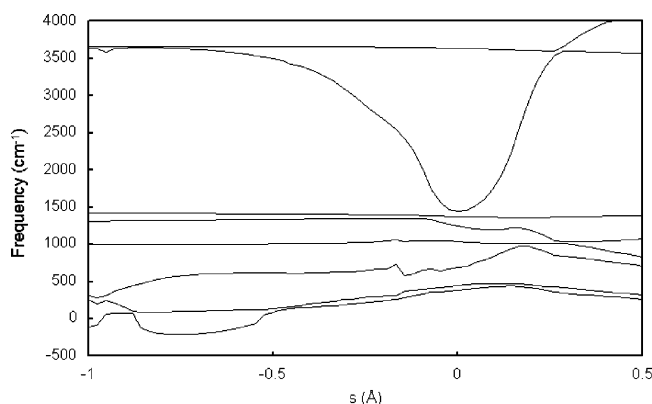
Figure 8. Frequencies calculated with M05-2X/MG3S for reaction 1b as functions of the reaction coordinate s, which is the signed distance along the reaction path from the saddle point. These frequencies are based on the RODS scheme with redundant internal coordinates.

significantly at low temperature. Therefore, from the small set of data that is available, it has been concluded that the values from Baldwin *et al.* at higher temperature are more likely to be reliable than those of Gorse and Volman. To match the rate coefficients of Baldwin *et al.*, a VTST-ISPE calculation was carried out where the barrier height was adjusted to the upper limit of the benchmark calculations, which is 10.4 kcal/mol. The energy of reaction was set to the best estimate of −16.4 kcal/mol, and the resulting calculation is labeled 10.4/−16.4 M05-2X/MG3S. The rate coefficients are listed in Table 14 and plotted in Figure 7. The $V_{MEP}(s)$ and $\Delta V_a^G(s)$ curves are shown in Figure S2 of the Supporting Information. The 10.4/−16.4 M05-2X/MG3S rate coefficients are in excellent agreement with the values obtained by Baldwin *et al.*

3.5. Rate Coefficient Calculations for the Total Reaction Rate. Finally, the total forward rate coefficients for reactions 1a and 1b are calculated in two ways: (i) by adding together the MPW1B95/MG3 calculation for 1a and the 10.4/−16.4
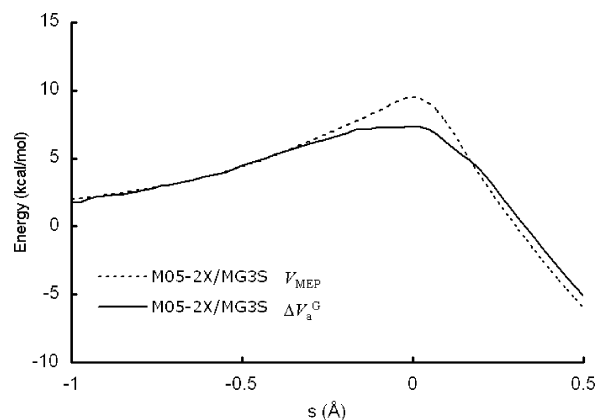
Figure 9. $V_{MEP}(s)$ and $\Delta V_a^G(s)$ with M05-2X/MG3S for reaction 1b as functions of the reaction coordinate s, which is the signed distance along the reaction path from the saddle point.

M05-2X/MG3S calculation for 1b, and (ii) by adding together the 4.6/−71.17 PW6B95/DIDZ calculation for 1a and the 10.4/−16.4 M05-2X/MG3S calculation for 1b. These sums are shown in the last two columns of Table 14. Recall that set i corresponds to a barrier height of 6.2 kcal/mol for reaction 1a to agree with the experiments of Gorse and Volman, Baldwin *et al.*, and Albers *et al.*, whereas set ii corresponds to a barrier height of 4.6 kcal/mol for reaction 1a to agree with the experiments by Klemm *et al.* Both sets of rate coefficients correspond to a reaction 1b of 10.4 kcal/mol to agree with the experiments of Baldwin. The calculated rate coefficients for 1a + 1b are plotted in Figure 10. Table 14 clearly shows that reaction 1a is the dominant reaction for all temperatures considered and that k_1 is only slightly larger than k_{1a}.

3.6. MRCM Estimates for Barrier Heights. *3.6.1. Reaction 1a.* The MRMP2 estimates for V_{1a} (see Table 3) with a series of correlation consistent basis sets and three different active spaces fall in the range 4.6−5.0 kcal/mol; these values show even greater agreement, from 4.8 to 4.9 kcal/mol, if one considers only the barriers at the consistently optimized geometries. The reaction barriers obtained using the MG3S basis set are more than 1 kcal/mol larger than those obtained with the both triple-ζ ANO and aug-cc-pVXZ (X = T, Q) series. A similar trend can be seen when comparing the results obtained using both single-reference and multireference coupled-cluster calculations (shown in Table 4). This indicates that MG3S is not a large enough basis set for converged wave function calculations for this system. The best estimate for a given method should be the one with the largest one-electron basis set and with the largest or best balanced active space; applying this criterion to Table 3 yields 4.8 kcal/mol. The infinite-basis-set limit of the MRMP2(CO:11/11) barrier height for reaction 1a was estimated by extrapolation from the cc-pVXZ (X = D, T, Q) basis sets of single-point energies at the MR-AQCC/MG3S reactant and saddle point geometries with a combined exponential-Gaussian function,[101] and this resulted in a nearly identical reaction barrier of 4.9 kcal/mol. A change of the active space of the reference CASSCF wavefunction from (CO:11/11) to the full valence active space (AP:15/11) and re-optimization of the structures at the same level (MRMP2 with the full-valence CASSCF reference wavefunction) resulted in little change of the calculated value of V_{1a}: in particular, Table 3 shows that the barrier height was either lowered by at most 0.2 kcal/mol or remained nearly unchanged. Similarly, the results for V_{1a} are fairly insensitive to a change from the CO(3:3) to the CO(11:11) active space. This confirms that both the CO
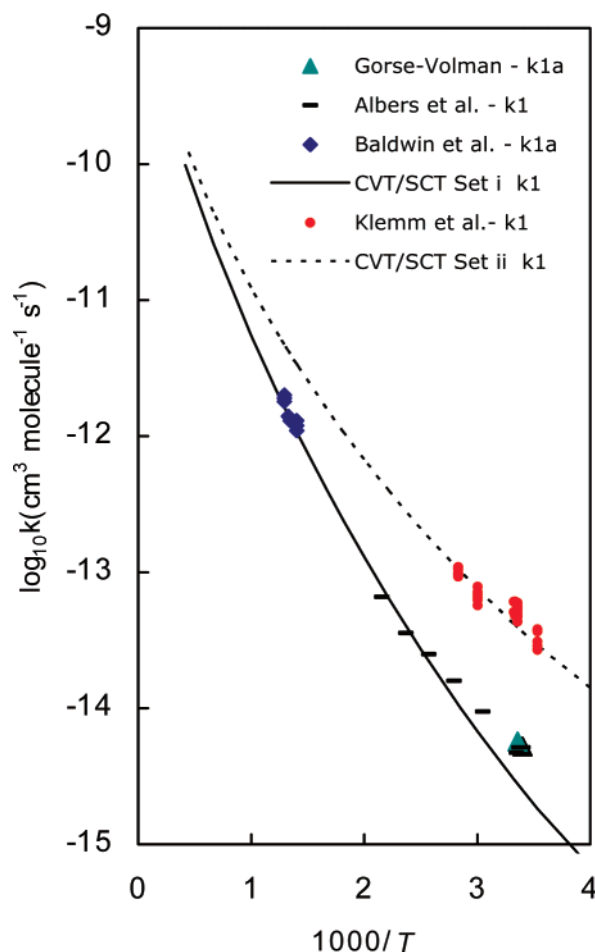
Figure 10. CVT/SCT rate coefficients k_1 (which denotes $k_{1a} + k_{1b}$) from Table 14 as compared to experimental values of k_{1a} and k_{1b} the rate coefficients.

(3:3) and CO(11:11) active spaces are well balanced for describing the corresponding region of the PES.

Because the results for reaction 1a are sensitive to diffuse functions (as a consequence of a rather large separation between the O-3 and H-5 atoms at the optimized transition structures of 1.590−1.670 Å (see Figure 1 and Table 5)), we repeated the MRMP2/aug-cc-pVDZ and MR-AQCC/aug-cc-pVDZ calculations with a doubly augmented basis set in which we added an extra set of diffuse s, p, and d functions on both oxygen atoms. Including these extra basis functions and re-optimizing the transition state and reactant geometries decreased the barrier only by about 0.1 kcal/mol, thus showing only a small sensitivity to extra diffuse functions.

The present study using the MR-AQCC method is restricted to only two one-electron basis sets and the (CO:3/3) active space. The MR-AQCC barrier heights are shown in Table 4, and the optimized geometrical parameters for reaction saddle points are listed in Tables 5 and 6. Even though the results presented here obtained using the MR-AQCC method are clearly incomplete (we believe that the results obtained using different electronic structure methods can only be compared at infinite basis set limit), they do provide some interesting information. In particular, they point out that the values for the forward barrier height of reaction 1a obtained by the MR-AQCC calculations with a CASSCF(CO:3/3) reference wave function is 7.3 kcal/mol with the MG3S basis set and 5.5 kcal/mol with the aug-cc-pVDZ basis set, whereas the corresponding values calculated at the CCSD(T)//MR-AQCC level are 7.5 and 5.8 kcal/mol. A similar change in the magnitude of V_{1a} calculated at these two

TABLE 15: Summary of Final Estimates (in kcal/mol) of Barrier Heights[a]

method	V_{1a}	V_{1b}
consensus benchmark-level single-reference multilevel results	6.5 ± 0.7	9.9 ± 0.4
CCSD(T)/CBS[b]	6.1	9.7
MRMP2/CBS[c]	4.8	9.1
estimated from experiments:		
Baldwin, Albers, Gorse *et al.*	6.2	10.4
Klemm *et al.*	4.6	n.a.[d]

[a] The barrier heights in this table (and in fact in the whole article) are saddle point heights relative to reactants; they exclude vibrational contributions. Such barrier heights are sometimes called classical barrier heights. [b] Complete basis set limit of single-reference CCSD(T) as estimated in section 3.7. [c] Complete basis set limit of multireference perturbation theory as estimated in section 3.6. [d] n.a. denotes not available.

levels with a change of the basis set is an indication that the barrier heights calculated using both CCSD(T) and AQCCSD theories at the infinite basis set limit would show no considerable discrepancy.

3.6.2. Reaction 1b. Consistently with the results of diagnostics presented in Section 3.2, the MRMP2 estimates for V_{1b} (8.9− 10.0 kcal/mol) fall in the same range as the single-reference benchmark-level results. Only the results obtained with (CO: 11/11) and (AP:15/11) active spaces are shown in Table 3 and the best available MRMP2 result for this reaction is 9.1 kcal/mol. The minimal (CO:3/3) active space, that by definition involves the σ_{OH} and σ_{OH}^* orbitals for this reaction, does not include the $\sigma_{OO},\sigma_{OO}^*$ orbital pair of the OO bond. This orbital pair is a significant source of nondynamical correlation effects in HOOH; therefore not including it in the active space may result in an unbalanced description of the reactant and the saddle point region at the MRMP2 level. This effect may be compensated by a better description of electron correlation beyond the MRMP2 level, and in fact, Table 4 shows that MR-AQCC-(CO:3/3) calculations give barrier heights within 0.4−0.7 kcal/mol of MRMP2(CO:11/11) calculations with the same one-electron basis sets, whereas Table 3 shows that MRMP2(CO: 3/3)/MG3S, which is not recommended, gives a value of V_{1b} that is 1.1 kcal/mol lower than MRMP2(CO:11/11) with the same basis set.

3.7. Single-Reference//Multireference Correlation Methods for Barrier Heights. Table 4 also includes the results of single-point energy calculation using the single-reference coupled-cluster method CCSD(T) at the MR-AQCC-optimized geometries. Because the UHF wavefunctions are severely spin-contaminated, we have repeated the calculations using the Kohn−Sham orbitals as the reference (see section 3.2), as well as the RHF orbitals as the reference. This resulted in a lowering of V_{1a} from 6.3 kcal/mol to about 6.1 kcal/mol. Furthermore, a change of the atomic orbital basis set from aug-cc-pVTZ to aug-cc-pVQZ left this barrier nearly unchanged, which is similar to the result we found for such a basis-set extension in MRMP2 calculations. This implies that a further improvement of the basis set (e.g., from aug-cc-pVQZ to aug-cc-pV5Z) will not significantly change the reaction barrier. This expectation leads to the conclusion that the CCSD(T) value for V_{1a} is approximately 6.1 kcal/mol.

3.8. Broad Assessment. A summary of the results of this study is given in Table 15. The best MRMP2 estimate for V_{1a} of 4.8 kcal/mol is in excellent agreement with the barrier height of 4.6 kcal/mol derived from the experimental measurement by Klemm *et al.* On the other hand, if reliable, the results of Gorse and Volman, Baldwin *et al.*, and Albers *et al.* would indicate

Reactions of H Atom with Hydrogen Peroxide

J. Phys. Chem. A, Vol. 111, No. 51, 2007 **13565**

that the MRMP2 barrier heights for reaction 1a are underestimated by about 1.4 kcal/mol. Although initial results of applications of the MRMP2 theory to investigation of reaction barrier heights were encouraging,[102–104] no systematic study has been presented so far that gives a reliable validation of the performance of MRCMs for chemical kinetics. Such a study would be valuable. Although it may seem more likely that MRMP2 would overestimate the barrier height by 0.2 kcal/mol than that it would underestimate the barrier height by 1.4 kcal/mol, which would give tentative support to the experiment of Klemm *et al.,* this would imply large errors (1.5–2.0 kcal/mol) in the barrier heights predicted by normally reliable single-reference methods, which would have to be explained by the multireference character of reaction 1a. It is important to keep in mind that whereas MRMP2 includes static correlation more completely than CCSD(T), the CCSD(T) method includes dynamic correlation more fully.

The results are more consistent for reaction 1b where MRMP2 yields 8.9–9.2 kcal/mol, and most of the benchmark-level single-reference methods are in the range 9.5–10.1 kcal/mol. Thus the spread of results is about a factor of 2 narrower for reaction 1b.

4. Conclusions

Rate coefficients measured for reactions $H + H_2O_2 \rightarrow H_2O + OH$ (1a) and $H + H_2O_2 \rightarrow HO_2 + H_2$ (1b) have been compared. The experimental rate coefficients determined by Klemm *et al.*[18] and those determined by Baldwin *et al.*[7–14] cannot both be correct. The reactions are studied here by a combination of electronic structure theory and direct dynamics. For reaction 1a the MPW1B95/MG3 density functional that yields a classical barrier height of 6.2 kcal/mol and a classical exoergicity of −71.2 kcal/mol leads to excellent agreement with the experiments by Baldwin *et al.*[7–14] as well as with the single-reference CCSD(T) barrier of 6.1 kcal/mol and with our consensus single-reference multicoefficient correlation method barrier height of 6.5 ± 0.7 kcal/mol. On the other hand, the barrier height obtained using the MRMP2 theory at the infinite-basis-set limit is about 1.3–1.7 kcal/mol lower. The MRMP2 barrier height of 4.8 kcal/mol is in favorable agreement with the barrier height that we infer from the measurements by Klemm *et al.*[18] This value represents the current best estimate of the zero-point-exclusive barrier for this reaction.

The rate coefficients for reaction 1b have been calculated using the M05-2X/MG3S level of theory with interpolated corrections; this yields a classical barrier height of 10.4 kcal/mol and a classical exoergicity of 16.4 kcal/mol. These agree with the experimentally determined rate coefficients of Baldwin *et al.*[7–14] and the conclusions[15,18] that $k_{1a} \gg k_{1b}$, as well as agreeing with an upper limit of the barrier given by high-level theory. The value of 10.4 kcal/mol thus should be considered as an upper limit of the barrier height for this reaction.

The total rate coefficient, k_1, has been determined as the sum of k_{1a} and k_{1b}. Two possible sets of recommended rate coefficients for k_{1a}, k_{1b}, and k_1 are listed in Tables 12–14 for a sequence of temperatures. Further work to determine which experiment and/or which levels of theory are reliable for this reaction would be valuable, and we hope that the present study serves to spur further study to resolve the uncertainties.

Supporting Information Available: A PDF file containing tables with optimized geometries and harmonic vibrational frequencies for reactants and products and CVT/SCT rate coefficients for reaction 1a using PBEKCIS*X*/MG3. Plots of $V_{MEP}(s)$ and ΔV_a^G. This material is available free of charge via the Internet at http://pubs.acs.org.

References and Notes

(1) Ulleberg, O.; Glockner, R. 14th World Hydrogen Energy Conference, June 9–13, 2002, Montreal.

(2) Rusek, J. J. *Future of Hydrogen Peroxide for Space Propulsion and Power Application*; Swift Enterprises: IN, 2000.

(3) Van Blargan, P.; Keller, O. *Int. J. Hydrogen Energy* **1998**, *23*, 603.

(4) Lee, D.; Hochgreb, S. *Int. J. Chem. Kinet.* **1998**, *30*, 385.

(5) Dixon-Lewis, G.; Williams, D. J. *Comprehensive Chem. Kinet.* **1977**, *17*, 1.

(6) Warnatz, J. *Combustion Chemistry*; Springer: New York, 1984.

(7) Baldwin, R. R.; Mayor, L. *Trans. Faraday Soc.* **1960**, *56*, 80.

(8) Baldwin, R. R.; Mayor, L.; Doran, P. *Trans. Faraday Soc.* **1960**, *56*, 93.

(9) Baldwin, R. R.; Mayor, L. *Trans. Faraday Soc.* **1960**, *56*, 103.

(10) Baldwin, R. R.; Jackson, D.; Walker, R. W.; Webster, S. J. *10th Combust. Symposium* **1965**, 423.

(11) Baldwin, R. R.; Jackson, D.; Walker, R. W.; Webster, S. J. *Trans. Faraday Soc.* **1967**, *63*, 1665.

(12) Baldwin, R. R.; Jackson, D.; Walker, R. W.; Webster, S. J. *Trans. Faraday Soc.* **1967**, *63*, 1676.

(13) Baldwin, R. R.; Brattan, D.; Tunnicliffe, B.; Walker, R. W.; Webster, S. J. *Combust. Flame* **1970**, *15*, 133.

(14) Baldwin, R. R.; Walker, R. W. *J. Trans. Faraday. Soc.* **1979**, *75*, 140.

(15) Albers, E. A.; Hoyermann, K.; Wagner, H. G.; Wolfrum, J. *13th Combust. Symp.* **1971**, 91.

(16) Gorse, R. A.; Volman, D. H. *J. Photochem.* **1974**, *3*, 115.

(17) Gorse, R. A.; Volman, D. H. *J. Photochem.* **1972**, *1*, 1.

(18) (a) Klemm, R. B.; Payne, W. A.; Stief, L. J. *First Int. Chem. Kinet. Symp.* **1975**, 61. (b) Michael, J. V.; Whytock, D. A.; Lee, J. H.; Payne, W. A.; Stief, L. J. *J. Chem. Phys.* **1977**, *67*, 3633.

(19) Tarchouna, Y.; Bahri, M.; Jaidane, N.; Lakhdar, Z. B. *J. Chem. Phys.* **2003**, *118*, 1189.

(20) Tarchouna, Y.; Bahri, M.; Jaidane, N.; Lakhdar, Z. B. *J. Mol. Struct.* **2006**, *758*, 53.

(21) Truhlar, D. G.; Garrett, B. C. *Acc. Chem. Res.* **1980**, *13*, 440.

(22) Truhlar, D. G.; Isaacson, A. D.; Garret, B. C. In *Theory of Chemical Reaction Dynamics*; Baer, M., Ed.; CRC Press: Boca Raton, FL, 1985; Vol. 3; p 65.

(23) Lu, D.-h.; Tucker, S. C.; Zhao, X. G.; González-Lafont, A.; Truong, T. N.; Maurice, D.; Liu, Y.-P.; Lynch, G. C.; Truhlar, D. G. In *Isotope Effects in Chemical Reactions and Photodissociation Processes*; Kaye, J. A., Ed.; ACS Symposium Series 502; American Chemical Society: Washington, DC, 1992; p 16.

(24) (a) Liu, Y.-P.; Lynch, G. C.; Truong, T. N.; Lu, d. h.; Truhlar, D. G.; Garrett, B. C. *J. Am. Chem. Soc.* **1993**, *115*, 2408. (b) Lu, D.-h.; Truong, T. N.; Melissas, V. S.; Lynch, G. C.; Liu, Y.-P.; Garrett, B. C.; Steckler, R.; Isaacson, A. D.; Rai, S. N.; Hancock, J. G.; Lauderdale, J. G.; Joseph, T.; and Truhlar, D. G. *Comput. Phys. Commun.* **1992**, *71*, 235.

(25) Fernandez-Ramos, A.; B. A. Ellingson; Garrett, B. C.; Truhlar, D. G. In *Reviews in Computational Chemistry*; Cundari, T. R.; Lipkowitz, K. B., Eds.; Wiley-VCH: Hoboken, NJ, 2007; Vol. 23, p 125.

(26) Baldridge, K. K.; Gordon, M. S.; Steckler, R.; Truhlar, D. G. *J. Phys. Chem.* **1989**, *93*, 5107.

(27) Gonzalez-Lafont, A.; Truong, T. N.; Truhlar, D. G. *J. Phys. Chem.* **1991**, *95*, 4618.

(28) Truong, T. N.; Lu, D.-h.; Lynch, G. C.; Liu, Y.-P.; Melissas, V. S.; Stewart, J. J. P.; Steckler, R.; Garrett, B. C.; Isaacson, A. D.; Gonzalez-Lafont, A.; Rai, S. N.; Hancock, G. C.; Joseph, T.; Truhlar, D. G. *Comput. Phys. Commun.* **1993**, *75*, 143.

(29) Liu, Y.-P.; Lu, D.-h.; Gonzalez-Lafont, A.; Truhlar, D. G.; Garrett, B. C. *J. Am. Chem. Soc.* **1993**, *115*, 7806.

(30) Truhlar, D. G. *Understanding Chemical Reactivity* **1995**, *16*, 229.

(31) Rossi, I.; Truhlar, D. G. *Chem. Phys. Lett.* **1995**, *233*, 231.

(32) Srinivasan, J.; Allison, T. C.; Schwenke, D. W.; Truhlar, D. G. *J. Phys. Chem. A* **1999**, *103*, 1487.

(33) Pu, J.; Truhlar, D. G. *J. Chem. Phys.* **2002**, *116*, 1468.

(34) Corchado, J. C.; Chuang, Y.-Y.; Coitino, E. L.; Ellingson, B. A.; Truhlar, D. G. GAUSSRATE - version 9.6; University of Minnesota: Minneapolis, 2007.

(35) Frisch, M. J. T., G. W.; Schlegel, H. B.; Scuseria, G. E.; Robb, M. A.; Cheeseman, J. R.; Montgomery, J. A., Jr.; Vreven, T.; Kudin, K. N.; Burant, J. C.; Millam, J. M.; Iyengar, S. S.; Tomasi, J.; Barone, V.; Mennucci, B.; Cossi, M.; Scalmani, G.; Rega, N.; Petersson, G. A.; Nakatsuji, H.; Hada, M.; Ehara, M.; Toyota, K.; Fukuda, R.; Hasegawa, J.; Ishida, M.; Nakajima, T.; Honda, Y.; Kitao, O.; Nakai, H.; Klene, M.; Li,

X.; Knox, J. E.; Hratchian, H. P.; Cross, J. B.; Bakken, V.; Adamo, C.; Jaramillo, J.; Gomperts, R.; Stratmann, R. E.; Yazyev, O.; Austin, A. J.; Cammi, R.; Pomelli, C.; Ochterski, J. W.; Ayala, P. Y.; Morokuma, K.; Voth, G. A.; Salvador, P.; Dannenberg, J. J.; Zakrzewski, V. G.; Dapprich, S.; Daniels, A. D.; Strain, M. C.; Farkas, O.; Malick, D. K.; Rabuck, A. D.; Raghavachari, K.; Foresman, J. B.; Ortiz, J. V.; Cui, Q.; Baboul, A. G.; Clifford, S.; Cioslowski, J.; Stefanov, B. B.; Liu, G.; Liashenko, A.; Piskorz, P.; Komaromi, I.; Martin, R. L.; Fox, D. J.; Keith, T.; Al-Laham, M. A.; Peng, C. Y.; Nanayakkara, A.; Challacombe, M.; Gill, P. M. W.; Johnson, B.; Chen, W.; Wong, M. W.; Gonzalez, C.; Pople, J. A. *Gaussian 03*, revision C.02; Gaussian, Inc: Wallingford, CT, 2004.

(36) Corchado, J. C.; Chuang, Y.-Y.; Fast, P. L.; W.-P., H.; Liu, Y.-P.; Lynch, G. C.; Nguyen, K. A.; Jackels, C. F.; Fernandez-Ramos, A.; Ellingson, B. A.; Lynch, B. J.; Melissas, V. S.; Villa, J.; Rossi, I.; Coitino, E. L.; Pu, J.; Albu, T. V.; Steckler, R.; Garrett, B. C.; Isaacson, A. D.; Truhlar, D. G. POLYRATE - version 9.6; Univeristy of Minnesota: Minneapolis, 2007.

(37) Corchado, J. C.; Coitino, E. L.; Chuang, Y.-Y.; Fast, P. L.; Truhlar, D. G. *J. Phys. Chem. A* **1998**, *102*, 2424.

(38) (a) Ellingson, B. A.; Lynch, V. A.; Mielke, S. L.; Truhlar, D. G. *J. Chem. Phys.* **2006**, *125*, 843050. (b) Pitzer, K. S. *J. Chem. Phys.* **1946**, *14*, 239. (c) Truhlar, D. G. *J. Comput. Chem.* **1991**, *12*, 1266. (d) Chuang, Y.-Y.; Truhlar, D. G. *J. Chem. Phys.* **2000**, *112*, 1221. (e) Califano, S. *Vibrational States*; Wiley: London, 1976; P. 210.

(39) Jackels, C. F.; Gu. Z.; Truhlar, D. G. *J. Chem. Phys.* **1995**, *102*, 3188.

(40) Chuang, Y.-Y.; Truhlar, D. G. *J. Chem. Phys.* **1997**, *107*, 83.

(41) (a) Villà, J.; Truhlar, D. G. *Theor. Chem. Acc.* **1997**, *97*, 317. (b) Gonzalez-Lafont, A.; Villà, J.; Lluch, J. M.; Bertrán, J.; Steckler, R.; Truhlar, D. G. *J. Phys. Chem. A* **1998**, *102*, 3420. (c) Fast, P. L.; Truhlar, D. G. *J. Chem. Phys.* **1998**, *109*, 3221.

(42) Cox, J. D.; Wagman, D. D.; Medvedev, V. A. *CODATA Key values for Thermodynamics*; Hemisphere: New York, 1989.

(43) Ruscic, B.; Wagner, A. F.; Harding, L. B.; Asher, R. L.; Feller, D.; Dixon, D. A.; Peterson, K. A.; Song, Y.; Qian, X.; Ng, C.-Y.; Liu, J.; Chen, W.; Schwenke, D. W. *J. Phys. Chem. A* **2002**, *106*, 2727.

(44) Gurvich, L. V.; Veyts, I. V.; Alcock, C. B. *Thermodynamic Properties of Individual Substances*, 4th ed.; Hemisphere: New York, 1989.

(45) Huber, K. P.; Herzberg, G. *Molecular Spectra and Molecular Structure IV. Constants of Diatomic Molecules*; Van Nostrand Reinhold: New York, 1979.

(46) Jacox, M. E. *J. Phys. Chem. Ref. Data Monograph* **1994**, *3*.

(47) (a) Koput, J.; Carter, S.; Handy, N. C. *J. Phys. Chem. A* **1998**, *102*, 6325. (b) Redington, R. L.; Olson, W. B.; Cross, P. C. *J. Chem. Phys.* **1962**, *36*, 1311.

(48) Shimanouchi, T. *Tables of Molecular Vibrational Frequencies, Consolidated Volume 1*; NSRDS NBS-39; NBS: Washington, DC, 1967.

(49) Curtiss, L. A.; Raghavachari, K.; Trucks, G. W.; Pople, J. A. *J. Chem. Phys.* **1991**, *94*, 7221.

(50) Curtiss, L. A.; Raghavachari, K.; Redfern, P. C.; Rassolov, V. A.; Pople, J. A. *J. Chem. Phys.* **1998**, *109*, 7764.

(51) Curtiss, L. A.; Raghavachari, K.; Redfern, P. C.; Pople, J. A. *J. Chem. Phys.* **1998**, *114*, 108.

(52) Ochterski, J. W.; Petersson, G. A.; Montgomery, J. A. *J. Chem. Phys.* **1996**, *104*, 2598.

(53) Ochterski, J. W.; Petersson, G. A.; Montgomery, J. A.; Frisch, M. J. *J. Chem. Phys.* **1999**, *110*, 2822.

(54) Fast, P. L.; Sanchez, M. L.; Truhlar, D. G. *Chem. Phys. Lett.* **1999**, *306*, 407.

(55) Lynch, B. J.; Zhao, Y.; Truhlar, D. G. *J. Phys. Chem. A* **2005**, *109*, 1643.

(56) Fast, P. L.; Corchado, J. C.; Sanchez, M. L.; Truhlar, D. G. *J. Phys. Chem. A* **1999**, *103*, 5129.

(57) Zhao, Y.; Rodgers, J. M.; Lynch, B. J.; Gonzalez-Garcia, N.; Pu, J.; Chuang, Y.-Y., Ellingson, B. A., Truhlar, D. G. MULTILEVEL - version 4.2; University of Minnesota: Minneapolis, 2006.

(58) Roos, B. O.; Taylor, P. *Chem. Phys.* **1980**, *48*, 157−173.

(59) Werner, H.-J.; Knowles, P. J. *J. Chem. Phys.* **1985**, *82*, 5053.

(60) Ruedenberg, K.; Schmidt, M. W.; Gilbert, M. M.; Elbert, S. T. *Chem. Phys.* **1982**, *71*, 41.

(61) Pulay, P.; Hamilton, T. P. *J. Chem. Phys.* **1987**, *88*, 4926.

(62) Anglada, J. M.; Olivella, S.; Sole, A. *J. Phys. Chem. A* **2007**, *111*, 1695.

(63) See, e.g.: Shaik, S.; Shurki, A. *Angew. Chem.* **1999**, *38*, 586.

(64) Hirao, K. *Chem. Phys. Lett.* **1992**, *190*, 374.

(65) Hirao, K. *Chem. Phys. Lett.* **1992**, *196*.

(66) Hirao, K. *Chem. Phys. Lett.* **1993**, *201*, 59.

(67) Hirao, K. *Int. J. Quantum Chem.* **1992**, *26*.

(68) Schmidt, M. W.; Baldridge, K. K.; Boatz, J. A.; Elbert, S. T.; Gordon, M. S.; Jensen, J.; Koseki, S.; Matsunaga, N.; Nguyen, K. A.; Su, S.; Windus, T. L.; Dupuis, M.; Montgomery, J. A. *J. Comput. Chem.* **1993**, *14*, 1347.

(69) Szalay, P. G.; Bartlett, R. J. *Chem. Phys. Lett.* **1993**, *214*, 481. Szalay, P. G., Bartlett, R. J. *J. Chem. Phys.* **1995**, *103*, 3600.

(70) Lischka, H.; Shepard, R.; Shavitt, I.; Pitzer, R. M.; Dallos, M.; Müller, T.; Szalay, P. G.; Brown, F. B.; Ahlrichs, R.; Böhm, H. J.; Chang, A.; Comeau, D. C.; Gdanitz, R.; Dachsel, H.; Ehrhardt, C.; Ernzerhof, M.; Höchtl, P.; Irle, S.; Kedziora, G.; Kovar, T.; Parasuk, V.; Pepper, M. J. M.; Scharf, P.; Schiffer, H.; Schindler, M.; Schüler, M.; Seth, M.; Stahlberg, E. A.; Zhao, J.-G.; Yabushita, S.; Zhang, Z.; Barbatti, M.; Matsika, S.; Schuurmann, M.; Yarkony, D. R.; Brozell, S. R.; Beck, E. V.; Blaudeau, J.-P. *COLUMBUS, an ab initio electronic structure program*, release 5.9.6; 2006.

(71) Lynch. B. J.; Zhao, Y.; Truhlar, D. G. *J. Phys. Chem. A* **2003**, *107*, 1384.

(72) Hehre, W. J.; Radom. L.; Shleyer, P. v. R.; Pople, J. A. *Ab Initio Molecular Orbital Theory*; Wiley: New York, 1086.

(73) Dunning, T. H., Jr. *J. Chem. Phys.* **1989**, *90*, 1007.

(74) Kendall, R. A.; Dunning, T. H., Jr.; Harrison, R. J. *J. Chem. Phys.* **1992**, *96*, 6796.

(75) Woon, D. E.; Dunning, T. H., Jr. *J. Phys. Chem.* **1994**, *100*, 2975.

(76) Widmark, P. O.; Malmqvist, P. A.; Roos, B. *Theor. Chim. Acta.* **1990**, *77*, 291.

(77) Lischka, H.; Shepard, R.; Pitzer, R. M.; Shavitt, I.; Dallos, M.; Muller, T.; Szalay, P. G.; Kedziora, G. S.; Yabushita, S.; Zhang, Z. *Phys. Chem. Chem. Phys.* **2001**, *3*, 664.

(78) Lynch, B. J.; Fast, P. L.; Harris, M.; Truhlar, D. G. *J. Phys. Chem. A* **2000**, *104*, 4811.

(79) Zhao, Y.; Lynch, B. J.; Truhlar, D. G. *J. Phys. Chem. A* **2004**, *108*, 2715.

(80) Zhao, Y.; Truhlar, D. G. *J. Phys. Chem. A* **2004**, *108*, 6908.

(81) Zhao, Y.; Truhlar, D. G. *J. Chem. Theor. Comput.* **2005**, *1*, 415.

(82) Zhao, Y.; Truhlar, D. G. *J. Phys. Chem. A* **2005**, *109*, 5656.

(83) Zhao, Y.; Shultz, N. E.; Truhlar, D. G. *J. Chem. Phys.* **2005**, *123*, 161103.

(84) Zhao, Y.; Truhlar, D. G. *J. Chem. Theor. Comput.* **2006**, *2*, 364.

(85) Zhao, Y.; Truhlar, D. G. MN-GFM - version 3.0; University of Minnesota: Minneapolis, 2007.

(86) Schultz, N. E.; Zhao, Y.; Truhlar, D. G. *J. Phys. Chem. A* **2005**, *109*, 11127.

(87) Schultz, N. E.; Gherman, B. F.; Cramer, C. J.; Truhlar, D. G. *J. Phys. Chem. B* **2006**, *110*, 24030.

(88) (a) Lee, T. J.; Taylor, P. R. *Int. J. Quantum Chem. Symp.* **1989**, *23*, 199. (b) Lee, T. J.; Rice, J. E.; Scuseria, G. E.; Schaefer, H. F., III. *Theor. Chim. Act*a **1989**, *75*, 81. (c) Lee, T. J.; Head-Gordon, M.; Rendall, A. P. *Chem. Phys. Lett.* **1**995, *243*, 402.

(89) Becke, A. D. *Phys. Rev. A* **1988**, *38*, 3098.

(90) Lee, C.; Yang, W.; Parr, R. G. *Phys. Rev. B* **1988**, *37*, 785.

(91) Adamo, C.; Barone, V. *Chem. Phys. Lett.* **1997**, *274*, 242.

(92) Purvis, G. D.; Bartlett, R. J. *J. Chem. Phys.* **1982**, *76*, 1910.

(93) Cizek, J. *Adv. Chem. Phys.* **1969**, *14*, 35.

(94) Raghavachari, K.; Trucks, G. W.; Pople, J. A.; Head-Gordon, M. *Chem. Phys. Lett.* **1989**, *157*, 479.

(95) Raghavachari, K.; Anderson, J. B. *J. Phys. Chem.* **1996**, *100*, 12960.

(96) Kohn, W. *Rev. Mod. Phys.* **1998**, *71*, 1253.

(97) Szabo, A.; Ostlund, N. S. *Modern Quantum Chemistry: Introduction to Advanced Electronic Structure Theory*; Dover Publications, Inc: Mineola, NY, 1996.

(98) (a) Beran, G. J. O.; Gwaltney, S. R.; Head-Gordon, M. *Phys. Chem. Chem. Phys.* **2003**, *5*, 2488. (b) Villaume, S.; Daniel, C.; Strich, A.; Perera, S. A.; Bartlett, R. J. *J. Chem. Phys.* **2005**, *122*, 44313.

(99) Werner, H.-J.; Knowles, P. J.; Amos, R. D.; Bernhardsson, A.; Berning, A.; Celani, P.; Cooper, D. L.; Deegan, M. J. O.; Dobbyn, A. J.; Eckert, F.; Hampel, C.; Hetzer, G.; Korona, T.; Lindh, R.; Lloyd, A. W.; McNicholas, S. J.; Manby, F. R.; Meyer, W.; Mura, M. E.; Nicklass, A.; Palmieri, P.; Pitzer, R.; Rauhut, G.; Schutz, M.; Schumann, U.; Stoll, H.; Stone, A. J.; Tarroni, R.; Thorsteinsson, T. MOLPRO, 2002.6; University of Birmingham: Birmingham, 2002.

(100) Fast, P. L.; Corchado, J.; Sanchez, M. L.; Truhlar, D. G. *J. Phys. Chem. A* **1999**, *103*, 3139.

(101) Woon, D. E.; Dunning, T. H., Jr. *J. Chem. Phys.* **1994**, *101*, 8877.

(102) Roberto-Neto, O.; Machado, F. B. C.; Truhlar, D. G. *J. Chem. Phys.* **1999**, *111*, 10046.

(103) Tishchenko, O.; Vinckier, C.; Nguyen, M. T. *J. Phys. Chem. A* **2004**, *108*, 1268.

(104) Tishchenko, O.; Vinckier, C.; Ceulemans, A.; Nguyen, M. T. *J. Phys. Chem. A* **2005**, *109*, 6099.